Published OnlineFirst August 21, 2015; DOI: 10.1158/0008-5472.CAN-14-3497

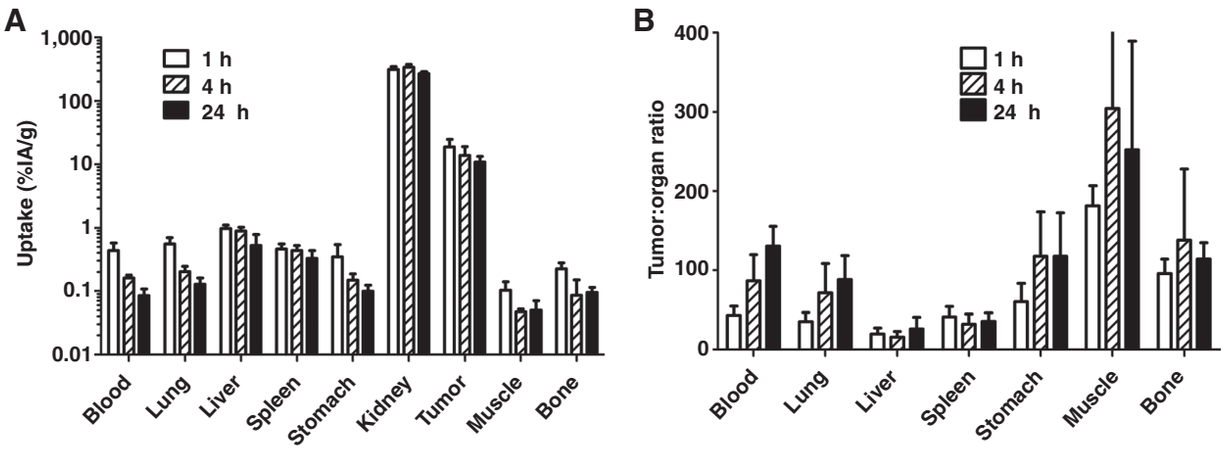

Figure 4.
Biodistribution (A) and tumor-to-organ ratios (B) of ^{111}In-DOTA-C-(HE)$_3$-ADAPT6 in mice bearing SKOV-3 xenografts. Data, mean ± SD ($n = 4$). Please note the logarithmic scale in A.

H_6-ADAPT6. Uptake in Ramos xenografts (0.112 ± 0.002 %IA/g) was significantly ($P < 0.05$) lower than uptake in SKOV-3 xenografts, on the same level as in muscles.

The biodistribution in normal organs (Fig. 4A) was characterized by rapid clearance from normal tissues except from kidneys and was in an excellent agreement with the data for NMRI mice. The tumor uptake was 18.7 ± 6.1, 13.9 ± 5.2, and 10.8 ± 2.5 %IA/g at 1, 4, and 24 hours p.i., respectively. Although the time points do not differ significantly ($P > 0.05$), there is a clear trend that tumor uptake decreases over time. Such biodistribution pattern provided high tumor-to-organ ratios already at 1 hour p.i. (Fig. 4B). For example, the tumor-to-blood ratio was as high as 43 ± 11 at this time point. At later time points, there was a significant ($P < 0.05$) increase only in tumor-to-blood and tumor-to-lung ratios.

Biodistribution and tumor-to-organ ratios of ^{68}Ga-DOTA-C-(HE)$_3$-ADAPT6 in BALB/C nu/nu mice bearing SKOV-3 (high HER2 expression) and LS174T (low HER2 expression) xenografts at 1 hour p.i. are shown in Tables 1 and 2. At both injected doses (1 or 15 μg), the uptake in SKOV-3 xenografts was much higher than in LS174T xenografts, which shows that tumor accumulation was dependent on target expression level. In both xenograft models, an increase of injected protein dose caused significant decrease of uptake, suggesting saturable uptake. At higher injected protein dose, the difference between xenografts with high and low HER2 expression was bigger (9.3-fold) than at lower dose (3.6-fold). Although uptake in SKOV-3 xenografts was lower at 15 μg, the tumor-to-organ ratios were not lower (Table 2).

Imaging

Experimental imaging (Fig. 5) confirmed the biodistribution results. The only normal organ with high uptake of radioactivity was kidney. No other organs were visualized. SKOV-3 xenografts with high HER2 expression were clearly visualized with a high contrast using 3 μg ^{111}In-DOTA-C-(HE)$_3$-ADAPT6. Saturation of receptors with DOTA-C-(HE)$_3$-ADAPT6 caused dramatic decrease of tumor uptake (Fig. 5A). PET imaging (Fig. 5B) demonstrated that xenografts with high (SKOV-3) and low (LS174T) HER2 expression could be easily distinguished using 15 μg ^{68}Ga-DOTA-C-(HE)$_3$-ADAPT6.

Discussion

Both theoretical calculations and experimental data (5, 7, 34) suggest that size reduction is the most promising way to increase imaging contrast provided by proteinaceous imaging agents.

Table 1. Biodistribution of ^{68}Ga-DOTA-C-(HE)$_3$-ADAPT6 in BALB/C nu/nu mice bearing SKOV-3 xenografts (high HER2 expression) and LS174T (low HER2 expression) at 1 hour p.i.

	SKOV3 xenografts		LS174T xenografts	
	1 μg	15 μg	1 μg	15 μg
Blood	0.59 ± 0.07	0.50 ± 0.06	0.60 ± 0.09	0.6 ± 0.2
Lung	0.70 ± 0.02	0.53 ± 0.06	0.67 ± 0.09	0.7 ± 0.2
Liver	1.7 ± 0.1	1.21 ± 0.05	1.8 ± 0.1	1.6 ± 0.1
Spleen	0.62 ± 0.05	0.50 ± 0.07	0.74 ± 0.07	0.56 ± 0.34
Stomach	0.63 ± 0.11	0.35 ± 0.07	0.54 ± 0.06	0.36 ± 0.09
Kidney	308 ± 24	277 ± 5	323 ± 27	311 ± 31
Tumor	10.3 ± 1.0[a,c]	8.4 ± 0.6[d]	2.9 ± 0.5[b]	0.9 ± 0.6
Muscle	0.18 ± 0.01	0.12 ± 0.02	0.14 ± 0.02	0.14 ± 0.03
Bone	0.5 ± 0.1	0.34 ± 0.07	0.5 ± 0.1	0.4 ± 0.1

NOTE: Data are presented as an average %IA/g and SD for four mice.
Difference was significant ($P < 0.05$) between:
[a]Injected dose of 1 and 15 μg in SKOV3 xenografts.
[b]Injected dose of 1 and 15 μg in LS174T xenografts.
[c]SKOV3 and LS174T xenografts at injected dose of 1 μg.
[d]SKOV3 and LS174T xenografts at injected dose of 15 μg.

Published OnlineFirst August 21, 2015; DOI: 10.1158/0008-5472.CAN-14-3497

Table 2. Tumor-to-organ ratios of ^{68}Ga-DOTA-C-(HE)$_3$-ADAPT6 in BALB/C nu/nu mice bearing SKOV-3 xenografts (high HER2 expression) and LS174T (low HER2 expression) at 1 hour p.i.

	SKOV3 xenografts		LS174T xenografts	
	1 μg	15 μg	1 μg	15 μg
Blood	17.5 ± 0.3	17 ± 2	4.8 ± 0.2	1.5 ± 0.8
Lung	15 ± 1	16 ± 1	4.3 ± 0.2	1.4 ± 0.7
Liver	6.0 ± 0.1	7.0 ± 0.4	1.6 ± 0.2	0.6 ± 0.4
Spleen	17 ± 2	17 ± 1	3.9 ± 0.4	2.1 ± 1.0
Stomach	16 ± 1	24 ± 4	5 ± 1	2 ± 1
Kidney	0.034 ± 0.005	0.030 ± 0.003	0.009 ± 0.002	0.003 ± 0.002
Muscle	56 ± 9	70 ± 6	21 ± 4	7 ± 4
Bone	20 ± 4	25 ± 4	7 ± 3	2 ± 1

NOTE: Data are presented as an average value and SD for four mice.

ADAPT (scaffold size 5.1 kDa without linkers and tags) has a size advantage in comparison with many other scaffold proteins, such as affibody molecules (7 kDa), designed ankyrin repeat proteins (14 kDa), anticalins (20 kDa), fibronectin domains (adnectins) (10 kDa), and VHHs (15 kDa). Knottins (4 kDa) are smaller, but they and many of the other scaffold proteins contain cysteines. The cysteine-free structure of ADAPT enables the use of oxidizing and reducing conditions during conjugation and labeling without affecting the structure of the domain. Moreover, the possibility to introduce a unique cysteine, as in this study, provides easy site-specific conjugation of chelators and other prosthetic groups that gives homogenous ADAPT conjugates. However, these potential advantages of ABD-based imaging agents could be realized only with three preconditions:

1. Generation of ABD derivatives with affinity in the range of 10 pmol/L to 10 nmol/L (35) to therapeutic targets should be possible;
2. Binding to albumin should be reduced to a level that permits rapid clearance from blood;
3. Off-target interaction of the scaffold should not cause any noticeable uptake in normal tissues.

An optimal affinity (K_D) for imaging agents should be in the range between 10 pmol/L and 10 nmol/L. If K_D is lower than 10 pmol/L (very high affinity), pharmacokinetics of the agent would depend heavily on blood flow or vascular permeability. Furthermore, if K_D is greater than 10 nmol/L, the off-rate will be too fast, and the retention at specific binding sites might be insufficient (35). This and previous studies (21, 23, 24) have demonstrated that selection of ADAPT binders with an optimal affinity to several therapeutic targets (HER2, HER3, and TNFα) is possible. This study has demonstrated that reduction of the affinity to albumin to a nonmeasurable level is also possible. The data from the first animal study (Fig. 2) demonstrated rapid clearance from blood. Furthermore, these data showed very low uptake in normal tissues (except kidneys), which suggests absence of noticeable off-target interactions. The high renal uptake is a general feature of all radiometal-labeled scaffold proteins, including nanobodies (36), affibody molecules (13–15), fibronectin domains (19), and designed ankyrin repeats (20). This uptake is caused by reabsorption from primary urine in proximal tubuli. After rapid internalization and proteolytic degradation, bulky hydrophilic radiometabolites get trapped inside proximal tubili cells. However, renal metastases are rather rare, and the well-defined shape of kidneys excludes false-positive findings. Moreover, our clinical study with affibody molecules suggests that high renal uptake does not prevent visualization of adrenal metastases and absorbed doses to kidneys permit multiple imaging procedures (12). Considerations concerning dosimetry aspects of high renal uptake are presented in Supporting Information. In addition, earlier we have shown for affibody molecules that the use of radiohalogen labels yields lipophilic radiometabolites, which "leak" rapidly from kidneys (11, 37). In the case of slow internalization by cancer cells, the use of radiohalogen labels has very little influence on tumor uptake of affibody molecules (11, 37). As internalization of ADAPT6 is also slow (Fig. 1D), the use of nonresidualizing radiohalogen labels may provide ADAPT-based

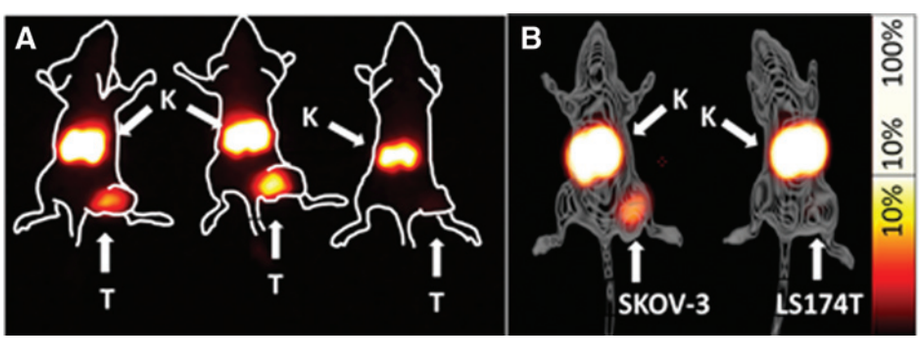

Figure 5.
Imaging of HER2 expression in xenografts using radiolabeled DOTA-C-(HE)$_3$-ADAPT6. A, gamma-camera imaging of SKOV-3 xenografts using ^{111}In-DOTA-C-(HE)$_3$-ADAPT6 (3 μg). Contours were derived from a digital photograph and superimposed over images to facilitate interpretation. A control animal (right) was injected with a saturating amount of nonlabeled ADAPT6. B, PET/CT imaging of SKOV-3 (high expression) and LS174T (low expression) xenografts using ^{68}Ga-DOTA-C-(HE)$_3$-ADAPT6. Injected protein dose was 15 μg. Arrows are pointing at tumors (T) and kidneys (K).

Published OnlineFirst August 21, 2015; DOI: 10.1158/0008-5472.CAN-14-3497

imaging agents with high uptake in tumors but low radioactivity retention in kidneys.

Both *in vivo* specificity tests (saturation and the use of HER2-negative xenografts) confirmed highly specific targeting of HER2-positive xenografts using ^{111}In-DOTA-C-$(HE)_3$-ADAPT6 (Fig. 3). Interestingly, the spleen uptake was increased in a saturation experiment. This might be due to weak cross-reactivity with other molecular targets expressed in the spleen or with a target that is taken up by the spleen. Such weak cross-reactivity is primarily manifested when a large amount of conjugate is injected (For more detailed consideration see Supplementary Information. Considerations concerning splenic uptake at high injected dose of ^{111}In-DOTA-C-$(HE)_3$-ADAPT6). Importantly, the uptake in HER2-positive xenografts exceeded uptake in negative ones by more than 160-fold. This demonstrated absence of an enhanced permeability and retention effect for ADAPTs, and excludes false-positive findings due to unspecific uptake in tumors. The uptake of the ADAPT in SKOV-3 xenografts (19 ± 6 %IA/g at 1 hour) was at the same level as for radiometal-labeled HER2-targeting affibody molecules (17 ± 2 %IA/g; ref. 38), and exceeded reported uptake for DARPins (8.3 ± 2.7 %IA/g; ref. 20) and nanobodies (4.7 ± 0.7 %IA/g; ref. 36) at the same time point in the same xenografts. The data concerning higher tumor uptake of smaller ADAPTs and affibody molecules in comparison with larger DARPins and nanobodies are consistent with a previous comparison with dimeric affibody molecules. It has been shown that the smaller monomers have higher tumor uptake than larger dimers (37). Together, these data suggest that the use of smaller scaffold proteins improves tumor targeting, presumably due to better extravasation. Importantly, clearance of ^{111}In-DOTA-C-$(HE)_3$-ADAPT6 was more rapid than clearance of, for example, affibody molecules. As a result, the highest tumor-to-organ ratios were reached very early (Fig. 4B), which enabled high-contrast imaging already at 1 hour p.i. (Fig. 5A). Ability to provide high-contrast images shortly after injection offers clear clinical and logistical advantages. Importantly, it permits the use of short-lived positron emitting radionuclides for labeling and therefore PET for imaging is feasible (Fig. 5B).

A rapid blood clearance in combination with high affinity might cause equal uptake of an imaging agent in tumors with high and low target expression. However, this limitation can be circumvented by increasing injected protein dose. We have shown this earlier for affibody molecules in preclinical models (39). In this study, an increase of the injected dose from 1 to 15 μg increased the difference in uptake in xenografts with low and high expression from 3-fold to more than 9-fold. This indicates that during possible clinical translation a dose-finding study should be performed to determine an optimal injected dose permitting clear discrimination between tumors with high and low target expression.

In conclusion, ADAPTs can be used as imaging agents that provide high-contrast PET imaging of HER2 expression in cancer shortly after injection. This shows that ADAPT is a very promising novel scaffold for development of imaging agents for personalized cancer treatment.

Disclosure of Potential Conflicts of Interest

J. Buijs is a CTO for Ridgeview Instruments AB. A. Orlova has ownership interest (including patents) and is a consultant/advisory board member for Affibody AB, Sweden. V. Tolmachev has ownership interest (including patents) and is a consultant/advisory board member for Affibody AB, Solna, Sweden. No potential conflicts of interest were disclosed by the other authors.

Authors' Contributions

Conception and design: S. Lindbo, J. Nilvebrant, M. Åstrand, A. Orlova, V. Tolmachev, S. Hober

Development of methodology: J. Garousi, S. Lindbo, J. Nilvebrant, M. Åstrand, H. Honarvar, A. Orlova, V. Tolmachev, S. Hober

Acquisition of data (provided animals, acquired and managed patients, provided facilities, etc.): J. Garousi, J. Nilvebrant, M. Sandström, H. Honarvar, A. Orlova, V. Tolmachev

Analysis and interpretation of data (e.g., statistical analysis, biostatistics, computational analysis): J. Garousi, S. Lindbo, J. Nilvebrant, M. Åstrand, J. Buijs, M. Sandström, H. Honarvar, A. Orlova, V. Tolmachev, S. Hober

Writing, review, and/or revision of the manuscript: J. Garousi, S. Lindbo, J. Nilvebrant, M. Åstrand, J. Buijs, M. Sandström, H. Honarvar, A. Orlova, V. Tolmachev, S. Hober

Administrative, technical, or material support (i.e., reporting or organizing data, constructing databases): V. Tolmachev

Study supervision: M. Sandström, V. Tolmachev, S. Hober

Grant Support

This research was financially supported by grants from the Swedish Cancer Society (grant 2012/354) and the Swedish Research Council (grants 521-2012-2228 and 621-2012-5088).

The costs of publication of this article were defrayed in part by the payment of page charges. This article must therefore be hereby marked *advertisement* in accordance with 18 U.S.C. Section 1734 solely to indicate this fact.

Received December 3, 2014; revised July 18, 2015; accepted July 23, 2015; published OnlineFirst August 21, 2015.

References

1. Tolmachev V, Stone-Elander S, Orlova A. Radiolabelled receptor-tyrosine-kinase targeting drugs for patient stratification and monitoring of therapy response: prospects and pitfalls. Lancet Oncol 2010;11:992–1000.
2. Behr TM, Béhé M, Wörmann B. Trastuzumab and breast cancer. N Engl J Med 2001;345:995–6.
3. Dijkers EC, Oude Munnink TH, Kosterink JG, Brouwers AH, Jager PL, de Jong JR, et al. Biodistribution of ^{89}Zr-trastuzumab and PET imaging of HER2-positive lesions in patients with metastatic breast cancer. Clin Pharmacol Ther 2010;87:586–92.
4. Gaykema SB, Brouwers AH, Lub-de Hooge MN, Pleijhuis RG, Timmer-Bosscha H, Pot L, et al. ^{89}Zr-bevacizumab PET imaging in primary breast cancer. J Nucl Med 2013;54:1014–8.
5. Jain RK. Physiological barriers to delivery of monoclonal antibodies and other macromolecules in tumors. Cancer Res 1990;50(3 Suppl):814s–819s.
6. Wester HJ, Kessler H. Molecular targeting with peptides or peptide-polymer conjugates: just a question of size? J Nucl Med 2005;46:1940–5.
7. Wittrup KD, Thurber GM, Schmidt MM, Rhoden JJ. Practical theoretic guidance for the design of tumor-targeting agents. Methods Enzymol 2012;503:255–68.
8. Chakravarty R, Goel S, Cai W. the "magic bullet" for molecular imaging? Theranostics 2014;4:386–98.
9. Binz HK, Amstutz P, Pluckthun A. Engineering novel binding proteins from nonimmunoglobulin domains. Nat Biotechnol 2005;23:1257–68.
10. Orlova A, Magnusson M, Eriksson TL, Nilsson M, Larsson B, Höidén-Guthenberg I, et al. Tumor imaging using a picomolar affinity HER2 binding affibody molecule. Cancer Res 2006;66:4339–48.
11. Orlova A, Wållberg H, Stone-Elander S, Tolmachev V. On the selection of a tracer for PET imaging of HER2-expressing tumors: direct comparison of a ^{124}I-labeled affibody molecule and trastuzumab in a murine xenograft model. J Nucl Med 2009;50:417–25.

12. Sörensen J, Sandberg D, Sandström M, Wennborg A, Feldwisch J, Tolmachev V, et al. First-in-human molecular imaging of HER2 expression in breast cancer metastases using the ^{111}In-ABY-025 affibody molecule. J Nucl Med 2014;55:730–5.
13. Tolmachev V, Rosik D, Wållberg H, Sjöberg A, Sandström M, Hansson M, et al. Imaging of EGFR expression in murine xenografts using site-specifically labelled anti-EGFR 111In-DOTA-Z EGFR:2377 Affibody molecule: aspect of the injected tracer amount. Eur J Nucl Med Mol Imaging 2010;37:613–22.
14. Orlova A, Malm M, Rosestedt M, Varasteh Z, Andersson K, Selvaraju RK, et al. Imaging of HER3-expressing xenografts in mice using a ^{99m}Tc(CO)$_3$-HEHEHE-Z HER3:08699 affibody molecule. Eur J Nucl Med Mol Imaging 2014;41:1450–9.
15. Orlova A, Hofström C, Strand J, Varasteh Z, Sandstrom M, Andersson K, et al. [99mTc(CO)$_3$]$^+$-(HE)$_3$-ZIGF1R:4551, a new Affibody conjugate for visualization of insulin-like growth factor-1 receptor expression in malignant tumours. Eur J Nucl Med Mol Imaging 2013;40:439–49.
16. Tolmachev V, Varasteh Z, Honarvar H, Hosseinimehr SJ, Eriksson O, Jonasson P, et al. Imaging of platelet-derived growth factor receptor β expression in glioblastoma xenografts using affibody molecule ^{111}In-DOTA-Z09591. J Nucl Med 2014;55:294–300.
17. Terwisscha van Scheltinga AG, Lub-de Hooge MN, Hinner MJ, Verheijen RB, Allersdorfer A, Hülsmeyer M, et al. *In vivo* visualization of MET tumor expression and anticalin biodistribution with the MET-specific anticalin ^{89}Zr-PRS-110 PET tracer. J Nucl Med 2014;55:665–71.
18. Ackerman SE, Currier NV, Bergen JM, Cochran JR. Cystine-knot peptides: emerging tools for cancer imaging and therapy. Expert Rev Proteomics 2014;11:561–72.
19. Hackel BJ, Kimura RH, Gambhir SS. Use of ^{64}Cu-labeled fibronectin domain with EGFR-overexpressing tumor xenograft: molecular imaging. Radiology 2012;263:179–88.
20. Zahnd C, Kawe M, Stumpp MT, de Pasquale C, Tamaskovic R, Nagy-Davidescu G, et al. Efficient tumor targeting with high-affinity designed ankyrin repeat proteins: effects of affinity and molecular size. Cancer Res 2010;70:1595–1605.
21. Nilvebrant J, Hober S. The albumin-binding domain as a scaffold for protein engineering. Comput Struct Biotechnol J 2013;6:e201303009.
22. Tolmachev V, Orlova A, Pehrson R, Galli J, Baastrup B, Andersson K, et al. Radionuclide therapy of HER2-positive microxenografts using a ^{177}Lu-labeled HER2-specific Affibody molecule. Cancer Res 2007;67:2773–82.
23. Nilvebrant J, Alm T, Hober S, Löfblom J. Engineering bispecificity into a single albumin-binding domain. PLoS ONE 2011;6:e25791.
24. Nilvebrant J, Astrand M, Löfblom J, Hober S. Development and characterization of small bispecific albumin-binding domains with high affinity for ErbB3. Cell Mol Life Sci 2013;70:3973–85.
25. Giordano SH, Temin S, Kirshner JJ, Chandarlapaty S, Crews JR, Davidson NE, et al. Systemic therapy for patients with advanced human epidermal growth factor receptor 2-positive breast cancer: American Society Of Clinical Oncology Clinical Practice Guideline. J Clin Oncol 2014;32:2078–99.
26. Wolff AC, Hammond ME, Hicks DG, Dowsett M, McShane LM, Allison KH, et al. Recommendations for human epidermal growth factor receptor 2 testing in breast cancer: American Society of Clinical Oncology/College of American Pathologists clinical practice guideline update. J Clin Oncol 2013;31:3997–4013
27. Natali PG, Nicotra MR, Bigotti A, Venturo I, Slamon DJ, Fendly BM, et al. Expression of the p185 encoded by HER2 oncogene in normal and transformed human tissues. Int J Cancer 1990;45:457–61.
28. Nilvebrant J, Åstrand M, Georgieva-Kotseva M, Björnmalm M, Löfblom J, Hober S. Engineering of bispecific affinity proteins with high affinity for ERBB2 and adaptable binding to albumin. PLoS ONE 2014;9:e103094.
29. Tolmachev V, Tran TA, Rosik D, Sjöberg A, Abrahmsén L, Orlova A. Tumor targeting using Affibody molecules: interplay of affinity, target expression level and binding site composition. J Nucl Med 2012;53:953–60.
30. Hofstrom C, Orlova A, Altai M, Wangsell F, Graslund T, Tolmachev V. Use of a HEHEHE purification tag instead of a hexahistidine tag improves biodistribution of affibody molecules site-specifically labeled with ^{99m}Tc, ^{111}In, and ^{125}I. J Med Chem 2011;54:3817–26.
31. Tolmachev V, Velikyan I, Sandström M, Orlova A. A HER2-binding Affibody molecule labelled with 68Ga for PET imaging: direct *in vivo* comparison with the 111In-labelled analogue. Eur J Nucl Med Mol Imaging 2010;37:1356–67.
32. Björkelund H, Gedda L, Barta P, Malmqvist M, Andersson K. Gefitinib induces epidermal growth factor receptor dimers which alters the interaction characteristics with 125I-EGF. PLoS ONE 2001;6:e24739.
33. Wållberg H, Orlova A. Slow internalization of anti-HER2 synthetic affibody monomer 111In-DOTA-ZHER2:342-pep2: implications for development of labeled tracers. Cancer Biother Radiopharm 2008;23:435–42.
34. Wållberg H, Ståhl S. Design and evaluation of radiolabeled tracers for tumor imaging. Biotechnol Appl Biochem 2013;60:365–83.
35. Eckelman WC, Kilbourn MR, Mathis CA. Discussion of targeting proteins *in vivo*: *in vitro* guidelines. Nucl Med Biol 2006;33:449–51.
36. Vaneycken I, Devoogdt N, Van Gassen N, Vincke C, Xavier C, Wernery U, et al. (2011) Preclinical screening of anti-HER2 nanobodies for molecular imaging of breast cancer. FASEB J 2011;25:2433–46.
37. Tolmachev V, Mume E, Sjöberg S, Frejd FY, Orlova A. Influence of valency and labelling chemistry on *in vivo* targeting using radioiodinated HER2-binding Affibody molecules. Eur J Nucl Med Mol Imaging 2009;36:692–701.
38. Ahlgren S, Orlova A, Wållberg H, Hansson M, Sandström M, Lewsley R, et al. Targeting of HER2-expressing tumors using 111In-ABY-025, a second-generation affibody molecule with a fundamentally reengineered scaffold. J Nucl Med 2010;51:1131–8.
39. Tolmachev V, Wållberg H, Sandström M, Hansson M, Wennborg A, Orlova A. Optimal specific radioactivity of anti-HER2 Affibody molecules enables discrimination between xenografts with high and low HER2 expression levels. Eur J Nucl Med Mol Imaging 2011;38:531–9